High Performance Ultrathin GaAs Solar Cells Enabled with Heterogeneously Integrated Dielectric Periodic Nanostructures

Sung-Min Lee,[†,∥] Anthony Kwong,[†,∥] Daehwan Jung,[§] Joseph Faucher,[§] Roshni Biswas,[‡] Lang Shen,[†] Dongseok Kang,[†] Minjoo Larry Lee,[*,§] and Jongseung Yoon[*,†,‡]

[†]Department of Chemical Engineering and Materials Science, University of Southern California, Los Angeles, California 90089, United States, [‡]Department of Electrical Engineering, University of Southern California, Los Angeles, California 90089, United States, and [§]Department of Electrical Engineering, Yale University, New Haven, Connecticut 06511, United States. [∥]S.-M.L. and A.K. contributed equally to this work.

ABSTRACT Due to their favorable materials properties including direct bandgap and high electron mobilities, epitaxially grown III–V compound semiconductors such as gallium arsenide (GaAs) provide unmatched performance over silicon in solar energy harvesting. Nonetheless, their large-scale deployment in terrestrial photovoltaics remains challenging mainly due to the high cost of growing device quality epitaxial materials. In this regard, reducing the thickness of constituent active materials under appropriate light management schemes is a conceptually viable option to lower the cost of GaAs solar cells. Here, we present a type of high efficiency, ultrathin GaAs solar cell that incorporates bifacial photon management enabled by techniques of transfer printing to maximize the absorption and photovoltaic performance without compromising the optimized electronic configuration of planar devices. Nanoimprint lithography and dry etching of titanium dioxide (TiO_2) deposited directly on the window layer of GaAs solar cells formed hexagonal arrays of nanoscale posts that serve as lossless photonic nanostructures for antireflection, diffraction, and light trapping in conjunction with a co-integrated rear-surface reflector. Systematic studies on optical and electrical properties and photovoltaic performance in experiments, as well as numerical modeling, quantitatively describe the optimal design rules for ultrathin, nanostructured GaAs solar cells and their integrated modules.

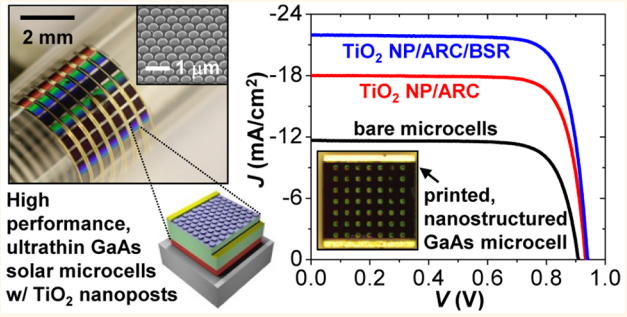

KEYWORDS: III–V solar cells · ultrathin gallium arsenide · nanophotonic light management · transfer printing · titanium dioxide

Single-crystalline III–V compound semiconductors such as gallium arsenide (GaAs) have been dominantly used for ultrahigh efficiency solar cells owing to a number of advantageous attributes including direct bandgap, tunable bandgap energy against the solar spectrum, high electron mobility, low temperature coefficient, as well as the ability to form monolithic multijunction devices.[1−7] Nevertheless, the prohibitively high cost for epitaxially growing device-quality single-crystalline materials, especially compared with silicon, has been the major barrier for the practical implementation of GaAs solar cells in terrestrial photovoltaics.[8−12] One viable means for lowering the cost of GaAs solar cells is to reduce the thickness of active materials as it can improve the economics of the cell fabrication by increasing the throughput of the epitaxial growth while reducing the consumption of high purity source materials.[13] However, the performance of such optically thin GaAs solar cells is intrinsically limited by the incomplete absorption of incident photons near the bandgap energy,[14−16] and optimized schemes of light management are therefore critically important to maintain the cost advantage from the reduced materials utilization. While many different kinds of nanophotonic schemes for scattering and light trapping have been explored in various solar cell systems with optically thin absorbers,[17−23] it has been particularly challenging to directly implement such photonic nanostructures

* Address correspondence to minjoo.lee@yale.edu, js.yoon@usc.edu.

Received for review July 18, 2015 and accepted September 6, 2015.

Published online September 16, 2015
10.1021/acsnano.5b05585

TABLE 1. Comparison of Photovoltaic Performance of Thin Film GaAs Solar Cells[a]

	absorber thickness (μm)[a]	J_{sc} (mA/cm^2)	V_{oc} (V)	FF	η (%)
Optically thin (this work)	**0.2**	**22.0**	**0.942**	**0.78**	**16.2**
Optically thin (Vandamme *et al.*)[13]	0.22	19.4	0.865	0.77	12.9
Optically thin (Yang *et al.*)[14]	0.3	24.5	1.000	0.78	19.1
Optically thick (Kayes *et al.*)[30]	-	29.7	1.122	0.87	28.8

[a] The thickness of emitter and base.

onto GaAs solar cells due to the stringent requirements of surface passivation, optical transparency, and high refractive index.[24−29] To date, several approaches have been successfully demonstrated using periodic[27] or randomly oriented[26,28] nanoscale features of the epitaxially grown $Al_{0.8}Ga_{0.2}As$,[27] amorphous titanium dioxide (TiO_2),[28] or indium tin oxide (ITO).[26] In these optically thick GaAs solar cells on growth wafers, the primary optical effect of the nanostructured layer was restricted to the suppression of front surface reflection due to the absorption loss in the substrate. On the other hand, introducing a reflective element on a back-side of GaAs solar cells is beneficial for improving the absorption of the near-bandgap photons in optically thin devices[13,14] or for collecting reemitted photons from radiative recombination.[30,31] Yang *et al.* demonstrated 19.1%-efficient, 300 nm-thick GaAs solar cells employing gold-coated, textured $Al_{0.52}In_{0.48}P$ as a reflective back scattering layer.[14] However, the need for a thick (~5 μm) $Al_{0.52}In_{0.48}P$ layer degraded the cost benefit associated with the use of thin active region. More recently, Vandamme *et al.* reported 12.9%-efficient, 220 nm-thick GaAs solar cells with a silver back mirror.[13] These approaches often involved a complete etching of the growth substrate after bonding to the module substrate, thereby limiting the cost-effectiveness, the spatial layout of solar cells, and the choice of substrate materials.

In this paper, we present alternative materials design and fabrication strategies for high performance ultrathin GaAs solar cells by simultaneously exploiting front-surface photonic nanostructure and rear-surface reflector in ways that allow the reuse of growth wafer. *Ex situ* fabricated nanoscale features of TiO_2 served as optically transparent diffractive elements implemented directly on the window layer of GaAs solar cells without compromising preexisting electronic configuration and optimized growth conditions. Transfer printing provided a practical means to engineer the front- and rear-surfaces of ultrathin, microscale GaAs solar cells in a synergistic fashion to maximize the performance, and also to distribute them over lightweight, low-cost substrates such as glass and polyethylene terephthalate (PET). The resulting GaAs solar cells with 200 nm-thick absorber (*i.e.*, emitter and base) printed on a PET substrate exhibited maximum one-sun efficiency of 16.2%, significantly improved compared with devices on the source wafer due to the combined optical effects of antireflection, diffraction, and light trapping, as well as the use of thin (~270 nm) bottom contact layer. Table 1 summarizes photovoltaic performance of the reported system in comparison with previous works on thin film GaAs solar cells. Systematic studies on optical, electrical, and morphological properties of GaAs solar cells in various device configurations together with optical and device modeling based on finite-difference time-domain and finite element methods provided insights into the underlying physics and materials science of the reported system, together with optimal design rules for nanostructured, transfer-printed GaAs solar cells.

RESULTS AND DISCUSSION

Figure 1a schematically illustrates the processing steps for our ultrathin, nanostructured GaAs solar cells, which build on our previously reported procedures with newly introduced schemes of TiO_2 nanofabrication.[10,11,19] The epitaxial stacks grown by molecular beam epitaxy (MBE) are composed of n^+-GaAs top contact (200 nm, Si-doped, 5×10^{18} cm^{-3}), n-$Al_{0.40}Ga_{0.60}As$ window (40 nm, Si-doped, 2×10^{18} cm^{-3}), n-GaAs emitter (50 nm, Si-doped, 2×10^{18} cm^{-3}), p-GaAs base (150 nm, Be-doped, 3×10^{17} cm^{-3}), p-$Al_{0.30}Ga_{0.70}As$ back-surface field (100 nm, Be-doped, 1×10^{19} cm^{-3}), p-GaAs bottom contact (1300 nm, Be-doped, 4×10^{19} cm^{-3}), and AlAs sacrificial layer (200 nm, undoped), grown on a semi-insulating GaAs wafer (Figure S1). The fabrication process began with the patterning of a top contact layer through a photolithography and wet chemical etching, followed by the deposition of TiO_2 (~170 nm) by radio frequency (RF) magnetron sputtering. Softimprint lithography, dry etching, and electron beam evaporation of metal formed hexagonally periodic Cr island arrays that serve as an etch mask for subsequent inductively coupled plasma reactive ion etching (ICP-RIE).[19] The resulting TiO_2 nanoposts (NPs) were patterned into a rectangular region within the cell boundary by photolithography and wet chemical etching. Additional steps of timed wet etching using photoresist masks formed a recessed bottom contact and isolated arrays of individual microscale (~500 × 500 μm^2) devices, followed by the metallization of n-type (AuGe/Ni/Au = 100/30/100 nm) and p-type

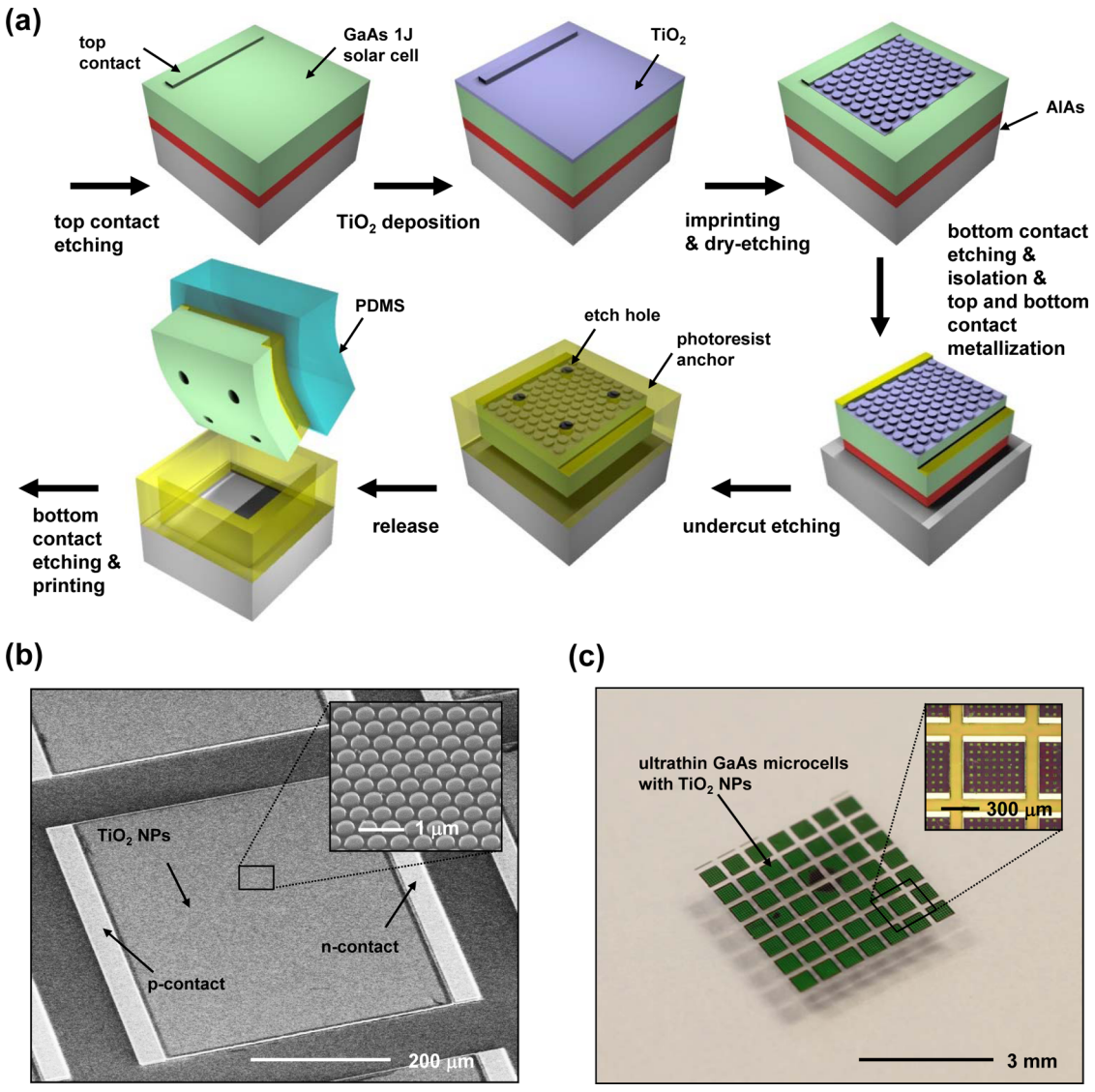

Figure 1. (a) Schematic illustration of the fabrication procedures for ultrathin (~610 nm) GaAs solar microcells heterogeneously incorporating the front-surface TiO_2 NPs. (b) Tilt-view SEM image of the resulting GaAs solar microcells with front-surface TiO_2 NPs on a source wafer. The inset presents a magnified view of the hexagonal arrays of TiO_2 NPs. (c) Photograph and optical micrograph (inset) images of 7 × 7 arrays of ultrathin GaAs solar microcells with TiO_2 NPs printed on a PET substrate.

(Cr/Au = 20/100 nm) ohmic contacts, and the selective removal of the sacrificial layer with photoresist anchor structures.[10,11,32,33] The undercut etched microcells with 200 nm-thick absorber layers were then released by an elastomeric stamp made of polydimethylsiloxane (PDMS) and printed over a glass or PET substrate using a photocured adhesive layer.[32,34] For a subset of samples before the printing step, the exposed bottom contact layer was additionally etched in a selective wet chemical etchant (*i.e.*, citric acid) to reduce its thickness from ~1300 to ~270 nm and therefore lower the parasitic loss of photogenerated carriers in the heavily doped layer. Complete details of the fabrication procedures appear in the Supporting Information. Figure 1b depicts a tilt-view scanning electron microscope (SEM) image of completed GaAs microcells with front-surface TiO_2 nanostructures (inset) on the growth wafer. A photographic image of printed arrays of nanostructured GaAs microcells on a PET substrate also appears in Figure 1c, where a diffractive green color is evident due to the integrated nanoscale features of TiO_2.

To identify optimal designs of TiO_2 nanostructures that can maximize the absorption of optically thin GaAs solar cells with the reduced thickness of the bottom contact layer (*i.e.*, ~ 270 nm), three-dimensional full-wave numerical modeling based on a finite-difference time-domain (FDTD) method was systematically performed over geometric parameters including period (p), diameter (D), and height (h) of the NPs, in which the photon absorption ($A(\lambda)$) only in the window, emitter,

base, and back-surface field (BSF) layers was considered as the source of generated photocurrents. More detailed information on numerical modeling and materials parameters is available in the Supporting Information (Figure S2). For the quantitative evaluation of solar cell performance with nanostructured GaAs solar cells, the calculated absorption was integrated over AM1.5G standard solar illumination (1000 W/m^2) to obtain integrated solar flux absorption, *S_abs*, given by[19,23]

$$S\_abs\ (\%) = \frac{\int_{400nm}^{873nm} \frac{\lambda}{hc} A(\lambda) I_{1.5G}(\lambda)\, d\lambda}{\int_{400nm}^{873nm} \frac{\lambda}{hc} I_{1.5G}(\lambda)\, d\lambda} \times 100 \quad (1)$$

where h, c, $I_{1.5G}$, and λ are Planck's constant, the speed of light, the standard solar irradiance (AM 1.5G; ASTM G-173), and wavelength, respectively. In all calculations, air (n = 1.0) and polymer (n = 1.5) were used as semi-infinite media above and below the printed GaAs microcell, respectively. Figure 2a presents a contour plot of calculated *S_abs* as a function of D and h of TiO_2 (n = 2.5) NPs at a fixed NP period (500 nm), from which the maximum integrated absorption and corresponding optimal geometries were identified at each NP period (*e.g.*, D = 330 nm, h = 150 nm at p = 500 nm). In a similar fashion, we examined the integrated absorption of nanostructured GaAs solar cells at various refractive indices of the dielectric NPs (Figures S3−S9), in which the absorption by the NP itself was assumed zero (*i.e.*, Im[n] = 0). Figure 2b shows a summary plot of the maximum *S_abs* as a function of NP period (p = 100−800 nm) at various refractive indices of NPs. As the refractive index of NP gets larger, a peak value of the maximum *S_abs* at an optimal period also increases but eventually decreases again when the refractive index is higher than the GaAs ($n \approx 4.0$) (Figure S10). The maximum integrated absorption of nanostructured GaAs solar cells at NP's refractive indices of 2.5, 3.0, 3.5, and 4.0 are 61.1, 62.2, 62.8, and 63.2%, respectively, all of which exceed the performance with optimal double layer antireflection coating (DLARC, TiO_2/SiO_2 = 60/100 nm, *S_abs* = 58.3%), optimal single layer ARC (SLARC, SiO_2 = 90 nm, *S_abs* = 52.7%), and no ARC (*S_abs* = 39.8%) (Figure S11). On the basis of these calculations, the use of TiO_2 as a material for the front-surface NP is well justified due to its high refractive index and minimum optical losses (*i.e.*, Im[n] $\approx$ 0) among currently available materials (Figure S12). The integrated absorption of GaAs solar cells with TiO_2 NPs can be further increased by incorporating a SLARC (SiO_2 = 70 nm (Figure S13)) over the TiO_2 layer and specular back-side reflector (s-BSR, silver) underneath the substrate to additionally suppress reflection losses at wavelengths below ~500 nm and trap weakly absorbed photons near the bandgap, respectively, which is captured in the corresponding absorption and reflectance spectra (Figure 2c). Notably, the values of *S_abs* for GaAs solar cells with TiO_2 NPs/SLARC (62.8% at p = 500 nm), TiO_2 NPs/s-BSR (63.9% at p = 400 nm), and TiO_2 NPs/SLARC/s-BSR (64.5% at p = 500 nm) are all higher than those of devices with DLARC/s-BSR (61.4%) mainly due to the strong effects of diffraction and light trapping in addition to the broad antireflection (Figures S14−S17). The contribution of respective optical processes to the absorption of ultrathin GaAs solar cells was also examined from the spatial distribution of absorbed power density (p_{abs}) normalized by the power (P_s) of the light source according to the following equation:[19]

$$p_{abs}(\vec{r}, \lambda)/P_s = (\pi c/\lambda)|\vec{E}(\vec{r}, \lambda)|^2 \mathrm{Im}[\varepsilon(\lambda)]/P_s \quad (2)$$

where $|\vec{E}|$ and ε are electric field intensity and the permittivity of constituent materials of GaAs solar cells, respectively. Figure 2d shows contour plots of normalized absorbed power density (p_{abs}/P_s) of printed bare GaAs solar cells (left), GaAs solar cells with DLARC/s-BSR (middle), and with TiO_2 NPs/SLARC/s-BSR (right), respectively, at wavelengths of 400, 550, 700, and 850 nm. The spatially modulated intensity distribution of absorbed power density is evident for GaAs solar cells with TiO_2 NPs compared to the other two cases as a result of nonzeroth order diffraction of the incident solar radiation. It is also noteworthy that the absorbed power density is more strongly concentrated near the pn-junction for devices incorporating TiO_2 NPs, which increases the probability of carrier collection and therefore contributes to the higher photogenerated current. The comparative advantage of TiO_2 NPs in light trapping over normal ARCs in ultrathin GaAs solar cells can be also appreciated in the calculated normalized total absorption ($A_t/(1 - R)$; $A_t = 1 - R - T$, total absorption (in the window, emitter, base, BSF, and bottom contact layers); R, reflectance; T, transmittance),[19,23] which provides the fraction of absorbed photons among those that enter the solar cell. As shown in Figure 2e, the normalized absorption of GaAs solar cells was significantly enhanced by adding TiO_2 NPs or both TiO_2 NPs and SLARC owing to the increased optical path length by diffraction and total internal reflection, while the implementation of DLARC makes negligible difference from the bare GaAs solar cell. On the other hand, the role and effectiveness of TiO_2 NPs are also closely related to the thickness of the underlying absorber layer and its absorption strength. To examine this aspect, we calculated the integrated absorption of a single layer of bare GaAs and GaAs with DLARC, DLARC/s-BSR, TiO_2 NPs, and TiO_2 NPs/SLARC/s-BSR, respectively (Figure 2f). As expected, in the optically thick regime (*e.g.*, >1 μm) of GaAs, the TiO_2 NPs mainly act as an ARC, where the *S_abs* of GaAs with TiO_2 NPs (red) is therefore comparable to that with DLARC (green). As the GaAs becomes thinner, however, GaAs with TiO_2 NPs starts to outperform

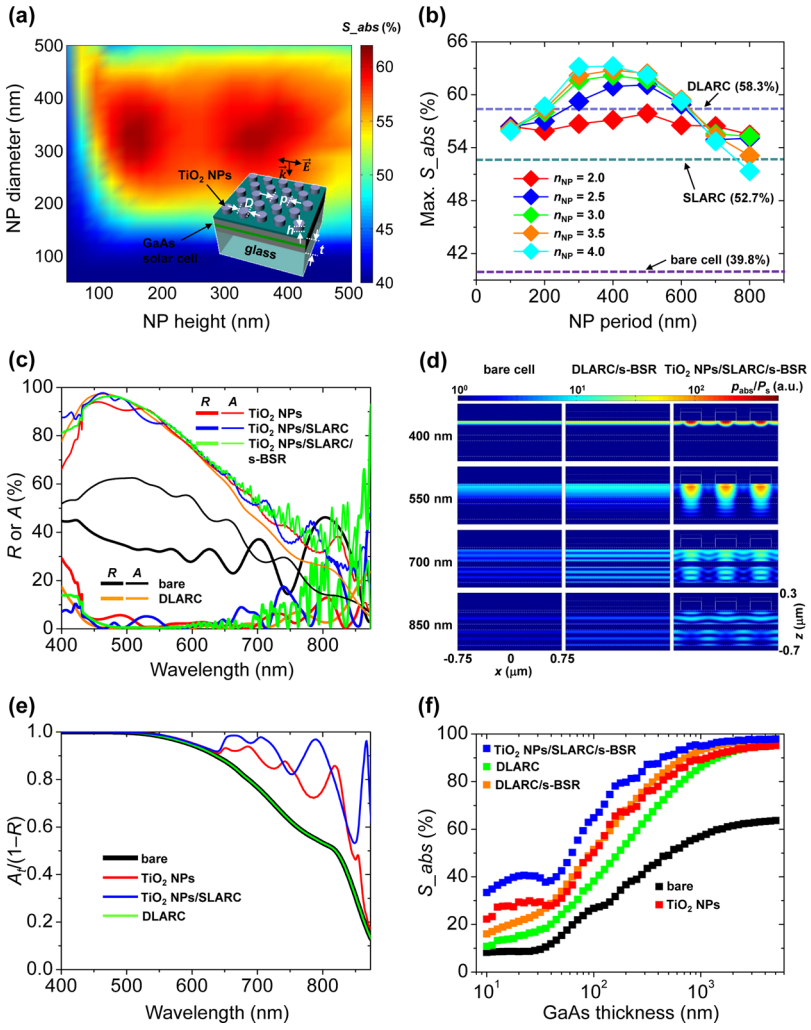

Figure 2. (a) Contour plot of the integrated solar flux absorption (*S_abs*) in window (n-$Al_{0.4}Ga_{0.6}As$, 40 nm), emitter (n-GaAs, 50 nm), base (p-GaAs, 150 nm), and back-surface field (BSF; p^+-$Al_{0.3}Ga_{0.7}As$, 100 nm) layers of a ultrathin GaAs solar cell incorporating TiO_2 NPs printed on a glass substrate as a function of diameter (*D*) and height (*h*) of NPs at a period (*p*) of 500 nm. The inset schematically illustrates a model for FDTD calculations. (b) Maximum integrated solar flux absorption of ultrathin GaAs solar cells with various refractive indices (*n* = 2.0−4.0) of NPs as a function of the NP period. The values of solar flux absorption for bare GaAs solar cell and GaAs solar cells with optimal single-layer antireflection coating (SLARC; t_{SiO2} = 90 nm) and with optimal double-layer antireflection coating (DLARC; t_{TiO2}/t_{SiO2} = 60/100 nm) are also presented for comparison. (c) Reflection (*R*, thick lines) and absorption (*A*, thin lines) spectra in window, emitter, base, and BSF layers for a bare GaAs solar cell (black) and GaAs solar cells with DLARC (orange), with TiO_2 NPs (*p* = 500 nm, *D* = 300 nm, *h* = 150 nm) (red), with TiO_2 NPs and SLARC (*p* = 500 nm, *D* = 350 nm, *h* = 350 nm, t_{SiO2} = 70 nm) (blue), and with TiO_2 NPs, SLARC, and a specular back-surface reflector (s-BSR) (*p* = 500 nm, *D* = 300 nm, *h* = 300 nm, t_{SiO2} = 70 nm) (green), where each configuration has its own optimal design to maximize the *S_abs*. (d) Contour plots of absorbed power per unit volume (p_{abs}) normalized by source power (P_s) for bare GaAs solar cell (left column), and GaAs solar cells with DLARC and s-BSR (middle column) and with TiO_2 NPs and both SLARC and s-BSR (right column) at wavelengths of 400, 550, 700, and 850 nm. (e) Normalized total absorption spectra ($A_t/(1 - R)$) of bare GaAs solar cell (black) and GaAs solar cells with DLARC (green), with TiO_2 NPs (red), and with TiO_2 NPs and SLARC (blue). (f) Integrated solar flux absorption of a single layer GaAs (black) and GaAs with DLARC (green), with DLARC and s-BSR (orange), with TiO_2 NPs (red), and with TiO_2 NPs and both SLARC and s-BSR (blue) as a function of the GaAs thickness.

GaAs with DLARC owing to the effect of the increased optical path length by nonzeroth order diffraction and light trapping. When combined with s-BSR and SLARC, the absorption of GaAs with TiO_2 NPs also well exceeds that with DLARC or DLARC/s-BSR in this optically thin regime. On the other hand, due to the fast saturation of *S_abs* with respect to the GaAs thickness, the corresponding integrated absorption normalized by the total cost (C_T) of epitaxial growth gradually increases with the decreasing thickness and reaches a maximum value in the thickness below 1 μm, in which the cost-normalized absorption of GaAs with TiO_2 NPs/SLARC/s-BSR is nearly two times higher than that of bare GaAs (Supporting Note in the Supporting Information, Figure S18).

Building on the outcomes of these computational studies, ultrathin GaAs solar microcells with near-optimal design of TiO_2 NPs (*p* = ∼500 nm, *D* = ∼370 nm, *h* = ∼140 nm) were fabricated on a glass substrate by transfer printing at various device configurations. Here,

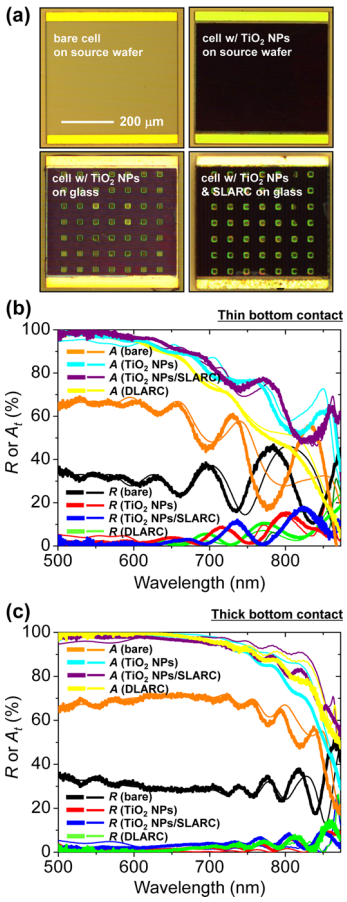

Figure 3. (a) Optical micrographs of GaAs solar microcells with (top-right) and without (top-left) TiO_2 NPs on the source wafer, and printed GaAs microcells on a glass substrate with TiO_2 NPs (bottom-left) and with TiO_2 NPs and SLARC (bottom-right). The bottom contact of the printed GaAs microcells was thinned down to ~270 nm by wet chemical etching after the release from the growth wafer. Measured (thick lines) and calculated (thin lines) reflectance (R) and total absorption (A_t) spectra of GaAs solar microcells printed on a glass substrate with (b) thin (~270 nm) and (c) thick (~1300 nm) bottom contact layers, respectively, including bare GaAs microcell (black/orange for R/A_t) and microcells with DLARC (green/yellow; t_{TiO2}/t_{SiO2} = 60/100 nm), with TiO_2 NPs (red/cyan; p = ~500 nm, D = ~370 nm, h = ~140 nm), and with TiO_2 NPs and SLARC (blue/purple; t_{SiO2} = ~70 nm).

a plain TiO_2 "base layer" (~30 nm) was introduced between the $Al_{0.40}Ga_{0.60}As$ window layer and TiO_2 NPs to minimize adverse effects upon the window layer during the fabrication of TiO_2 NPs, which makes little difference in optical properties compared with the case without the base layer as confirmed by the calculation (Figure S19). Figure 3a shows optical micrographs of GaAs microcells on the source wafer with and without TiO_2 NPs, printed GaAs microcells with TiO_2 NPs and TiO_2 NPs/SLARC (SiO_2 = ~70 nm), respectively. The GaAs microcell on the source wafer with TiO_2 NPs exhibited a black-colored surface, while the printed microcell with TiO_2 NPs appeared slightly brighter, possibly due to the incomplete antireflection in the short wavelength range as well as the reflection of longer wavelength photons from the bottom surface of the microcell. Depositing an additional layer of SiO_2 (*i.e.*, SLARC) yielded a darker surface and improved the antireflection behavior. The corresponding measured (thick line) and calculated (thin line) reflectance (R) and total absorption ($A_t = 1 - R - T$) spectra of printed ultrathin GaAs microcells with thin (~270 nm) and thick (~1300 nm) bottom contact layers are shown in Figure 3, panels b and c, respectively. For microcells having a thin bottom contact layer (Figure 3b), device configurations with TiO_2 NPs and TiO_2 NPs/SLARC exhibited similar antireflection behaviors to the case with DLARC in the wavelength range (λ = 500−873 nm) for measurements, while their absorption was noticeably higher due to the increased optical path length by diffraction and light trapping. For microcells with a thick bottom contact layer (Figure 3c), the increase of total absorber thickness resulted in reduced reflectance and increased absorption. However, the magnitude of absorption enhancement by TiO_2 NPs over DLARC is much smaller in cells with a thick bottom contact layer due to the reduced effectiveness of light trapping in the optically thick absorber as discussed in Figure 2f.

Although ultrathin GaAs microcells with a thick bottom contact layer can absorb more photons than those with a thin bottom contact layer, their photovoltaic performance is inferior to devices with a thin bottom contact layer. That is because absorbed photons in the heavily doped GaAs bottom contact layer makes little contribution to the photogenerated current due to the Auger recombination and severely restricted minority carrier diffusion length. To quantitatively examine the effect of the bottom contact thickness upon the device performance, the photovoltaic characteristics of GaAs microcells were numerically modeled using a device simulator based on a finite element method (FEM) (DEVICE 4.5, Lumerical Solutions). As illustrated in the calculated energy band structure of GaAs solar cells considered in this study (Figure 4a), the energy barrier at the BSF layer is partially responsible for the inhibited transport and collection of photogenerated electrons from the p-type bottom contact layer to the junction, in addition to the limited minority carrier lifetime arising from the high doping concentration. On the other hand, minority carriers generated in p^+-$Al_{0.3}Ga_{0.7}As$ BSF (*i.e.*, electrons) and n-$Al_{0.4}Ga_{0.6}As$ window (*i.e.*, holes) layers are able to diffuse to the junction and participate in the photocurrent generation due to the lack of such barriers. To quantitatively evaluate the contribution of photon absorption in each epitaxial layer to the current generation of printed GaAs microcells, we performed calculations to obtain the spatial distribution of the number of generated electron−hole pairs per unit volume and time ($g_{e\text{-}h}$) under AM1.5G standard solar illumination through the FDTD simulation assuming

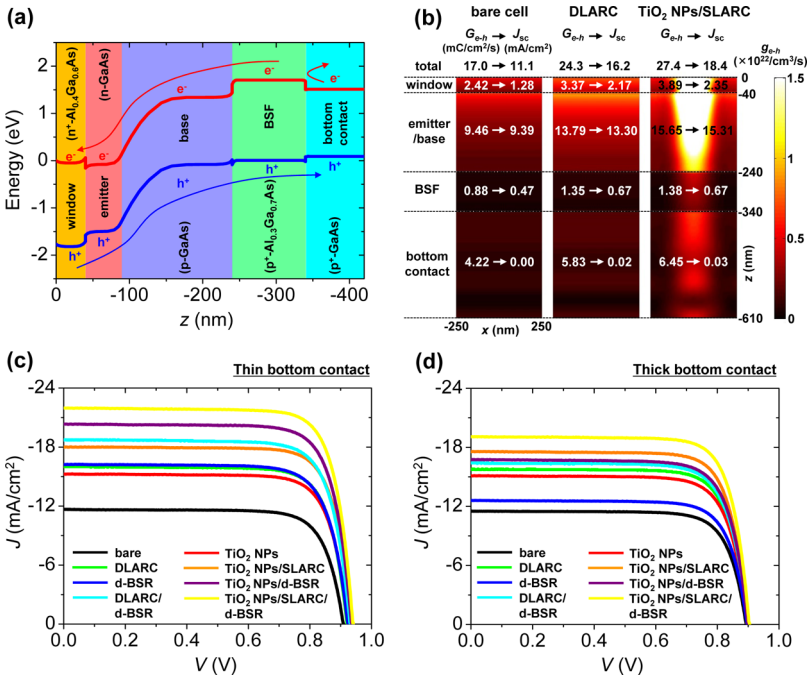

Figure 4. (a) Calculated energy band structure of an ultrathin GaAs solar cell as a function of the distance from the top surface of a window (n-$Al_{0.4}Ga_{0.6}As$) layer. (b) Contour plots of calculated number of generated electron−hole pairs per unit volume and time ($g_{e\text{-}h}$) in an ultrathin GaAs solar cells under AM1.5G standard solar illumination (1000 W/m^2) at various cell configurations (bare, DLARC, TiO_2 NPs/SLARC) with a thin (∼270 nm) bottom contact layer. Calculated values of generated charge density per unit area and time ($G_{e\text{-}h}$) and short-circuit current density (J_{sc}) in each epitaxial layer are also displayed for comparison. Representative current density (J)−voltage (V) curves of printed ultrathin GaAs solar microcells with (c) thin (∼270 nm) and (d) thick (∼1300 nm) bottom contact layers at various cell configurations, including bare microcell (black) and microcells with DLARC (green), with a diffuse back-surface reflector (d-BSR) (blue), with DLARC and d-BSR (cyan), with TiO_2 NPs (red), with TiO_2 NPs and SLARC (orange), with TiO_2 NPs and d-BSR (purple), and with TiO_2 NPs, SLARC, and d-BSR (yellow) measured under AM 1.5G standard solar illumination.

the generation of one electron−hole pair per one absorbed photon, which is given by

$$g_{e\text{-}h}(\vec{r}) = \int [(\lambda/hc)(p_{abs}(\vec{r},\lambda)/P_s)I_{1.5G}(\lambda)S_{inc}]\, d\lambda \quad (3)$$

where p_{abs}/P_s and S_{inc} denote normalized absorbed power density obtained from eq 2 and the area illuminated by the incident light source, respectively. The calculated distribution of $g_{e\text{-}h}$ as illustrated in the contour plot of Figure 4b was then imported into the FEM-based device simulator to obtain the short-circuit current density (J_{sc}) of the solar cell, where Auger (recombination coefficient = 7×10^{-30} cm^6/s for both electrons and holes in GaAs and $Al_xGa_{1-x}As$ (x = 0.3 and 0.4)) and radiative (recombination coefficient = 5×10^{-10} cm^3/s in GaAs and 1.4×10^{-20} cm^3/s in $Al_xGa_{1-x}As$ (x = 0.3 and 0.4)) recombinations, and ohmic contacts were assumed at room temperature with negligible surface and Shockley−Read−Hall recombinations. Subsequently, the calculated J_{sc} was compared with the integrated charge density per unit area and time ($G_{e\text{-}h}$) evaluated by

$$G_{e\text{-}h} = (1/S_{inc})\int_V g_{e\text{-}h}(\vec{r})\, dV \quad (4)$$

where the integration was performed over an entire range of the cell volume. The calculated $G_{e\text{-}h}$ provides the maximum photocurrent density from the absorbed photons without any parasitic losses. As expected, photogenerated carriers in the emitter and base layers mostly translated into the output current due to the relatively short distance to the junction and the built-in electric field, whereas those from the bottom contact layer rarely contributed due to severe recombination losses and the presence of an energy barrier (Figure 4b). Not surprisingly, minority carriers from the window and BSF layers made a partial contribution to the current generation. Such nonuniform collection efficiency of photogenerated carriers in each epitaxial layer of GaAs solar cells suggests that the spatial distribution of the absorbed photon flux can play an important role for maximizing the photovoltaic performance if the amount of total absorption is fixed. In this regard, GaAs solar cells with TiO_2 NPs/SLARC provide an additional advantage in absorption over the case of bare GaAs or GaAs with DLARC due to the effect of field confinement near the junction as illustrated in Figure 2d. Panels c and d of Figure 4 show the measured photovoltaic performance of printed GaAs microcells with thin (∼270 nm) and thick (∼1300 nm) bottom contact layers, respectively, at various cell configurations, where the data with a diffuse back-side reflector (d-BSR) are included. The data with a specular reflector (s-BSR)

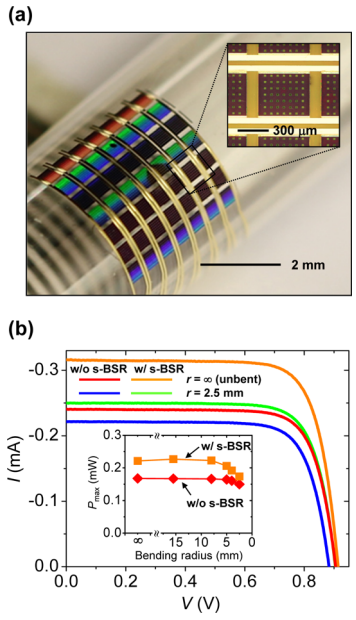

Figure 5. (a) Photographic image of the mechanically flexible solar module comprising 7 × 7 ultrathin GaAs solar microcells (cell size = ~500 × 500 μm^2, cell-to-cell spacing = ~100 μm) with front-surface TiO_2 NPs and thin (~270 nm) bottom contact layer on a PET substrate (inset: optical micrograph of the interconnected GaAs microcells). (b) Representative current (*I*)−voltage (*V*) curves of interconnected 7 microcells with or without a s-BSR at unbent and bent (bending radius (*r*) = 2.5 mm) states. The inset shows the corresponding maximum power of the interconnected microcells at various bending radii.

were also measured and are available in the Supporting Information (Figure S20, Tables S2 and S3). First of all, it is clearly shown that the TiO_2 NPs implemented on the window layer made no detrimental effects upon the device performance owing to the preserved efficacy of surface passivation, as supported by the unchanged open-circuit voltage (V_{oc}) and fill-factor (FF). For GaAs microcells with a thick bottom contact layer, the effect of the d-BSR is relatively limited as a result of high degrees of parasitic losses for photogenerated carriers in the bottom contact layer. The comparatively lower J_{sc} improvement (~30%) in microcells with TiO_2 NPs against bare microcells than in those with DLARC (~37%) is attributed to the incomplete coverage (~90%) of TiO_2 on the cell surface and associated reflection loss. The addition of a SLARC to TiO_2 NPs yielded considerably higher J_{sc} improvement (~54%) due to the broadened antireflection behavior as well as the full areal coverage of SLARC, which is also close to the calculated maximum enhancement of the *S_abs* (~58%). On the other hand, the performance of microcells with a thin bottom contact layer was more strongly enhanced by the d-BSR owing to the decreased level of recombination in the bottom contact layer. The experimental J_{sc} enhancement by the d-BSR is comparatively greater than the calculated absorption (*S_abs*) enhancement (*e.g.*, J_{sc}(d-BSR)/J_{sc}(bare) = 1.38, *S_abs*(s-BSR)/*S_abs*(bare) = 1.07 for bare GaAs; J_{sc}(NPs/d-BSR)/J_{sc}(NPs) = 1.33, *S_abs*(NPs/s-BSR)/*S_abs*(NPs) = 1.04 for nanostructured GaAs), due to the contribution of additional photon flux by the light that is incident on areas outside the printed microcells, reflected, and waveguided to the cell through a substrate and a printing medium. It is also notable that a diffuse BSR used in the measurements is more effective than a specular BSR used in the calculation for making such waveguiding effects and the indirect photon flux. As expected, the highest photovoltaic performance was obtained from microcells with a thin bottom contact layer and TiO_2 NPs/SLARC/d-BSR owing to the synergistic effects of antireflection, diffraction, light trapping, as well as reduced parasitic losses in the bottom contact layer, where the J_{sc}, V_{oc}, FF, and η were 22.0 mA/cm^2, 0.942 V, 0.78, and 16.2%, respectively, which is superior to other configurations such as GaAs microcells with a thin bottom contact and DLARC/d-BSR (J_{sc} = 18.7 mA/cm^2, V_{oc} = 0.932 V, FF = 0.77, η = ~13.5%) or with thick bottom contact and TiO_2 NPs/SLARC/d-BSR (J_{sc} = 19.1 mA/cm^2, V_{oc} = 0.906 V, FF = 0.78, η = ~13.4%). More details of the photovoltaic performance characteristics at various cell configurations are available in the Supporting Information (Figure S21, Tables S2 and S3).

The reported ultrathin (~610 nm) GaAs microcells are also an attractive device platform for constructing mechanically flexible solar modules due to the substantially reduced flexural rigidity.[35] Figure 5a shows a photographic image of 7 × 7 arrays of ultrathin GaAs microcells having a thin bottom contact layer and TiO_2 NPs printed on a PET (~50 μm) substrate, where microcells were connected in parallel by electron-beam evaporated metal (Cr/Ag/Au = 15/1000/30 nm) lines. As shown in the corresponding current (*I*)−voltage (*V*) curves of 7 parallel-connected microcells (Figure 5b), the performance of the flexible solar module remained invariant at the bending radius of as small as ~5 mm even without the encapsulation layer to implement neutral mechanical plane schemes.[10] Slight degradation of performance at bending radii below 5 mm is attributed to the decreased incident solar flux upon bending (Figure S22) as well as angle-dependent nature of diffraction-induced antireflection effect that degrades at large incidence angles. When a silver layer (~300 nm) as a specular BSR was introduced to the back surface of the PET substrate, the maximum output power was enhanced by ~32.0% at unbent states. However, its bent-state performance with a s-BSR decreased more steeply at bending radii below 5 mm possibly due to photons that are reflected by the BSR at off-normal angles and not captured by the microcells.

CONCLUSION

In conclusion, we studied cost-effective, high performance GaAs solar cells by exploiting bifacial photon management schemes that incorporate front-surface

dielectric photonic nanostructures and rear-surface specular or diffuse reflectors with 200 nm-thick absorber layers. The hexagonally periodic TiO_2 nanoposts implemented directly on the window layer of ultrathin GaAs solar cells, combined with the BSR on the rear surface of the module substrate, provided synergistic effects of antireflection, diffraction, and light trapping, which allowed superior absorption and enhanced photovoltaic performance to devices with conventional DLARC while drastically reducing the thickness of the epitaxial materials. The ultrathin GaAs microcells printed on a flexible PET substrate, when configured with TiO_2 NPs/SLARC/d-BSR, exhibited maximum efficiency of ~16.2% and stable operation at bending radius of as small as ~5 mm. The materials design and fabrication strategies reported in this study represents important progress toward cost-competitive III−V solar cells in terrestrial applications. We anticipate similar optical and electronic design principles can be readily applicable to other III−V materials systems and/or multijunction devices. Epitaxial and optical designs that simultaneously maximize light trapping, photon recycling, and charge carrier collection of ultrathin GaAs solar cells are interesting topics for future studies.

METHODS

Fabrication of Ultrathin GaAs Solar Microcells with Front-Surface TiO_2 Nanoposts. With epitaxial stacks of GaAs solar cells grown by MBE, the fabrication of ultrathin GaAs solar microcells with TiO_2 NPs started with the patterning of a GaAs top contact layer to expose a window layer except the region for a n-type ohmic contact by wet chemical etching in the solution of citric acid ($C_6H_8O_7$) and hydrogen peroxide (H_2O_2) (4:1 by volume). After the deposition of TiO_2 (~170 nm) by RF magnetron sputtering (Orion 5, AJA International), soft-imprint lithography and oxygen reactive ion etching (RIE, Plasmalab) of SU-8 were carried out to form hexagonally periodic nanohole arrays, followed by electron beam evaporation (Temescal) and liftoff of Cr (~8 nm). The resulting Cr islands were then used as a mask for inductively coupled plasma reactive ion etching (ICP-RIE, Plasmalab system 100, Oxford) to yield hexagonally periodic TiO_2 NPs, followed by the wet chemical etching of Cr and TiO_2 (CR-7, Cyantek for Cr etching, HF/H_2O; 1:10 by volume for TiO_2 etching) to produce TiO_2 NPs lithographically defined within the cell area. Additional steps of photolithography and wet chemical etching in phosphoric acid (H_3PO_4)/H_2O_2/H_2O (1:12:11 by volume) and $C_6H_8O_7$/H_2O_2 (20:1 by volume) formed a recessed bottom contact and isolated arrays of microcells (~500 × 500 μm^2). Subsequently, n-type (AuGe/Ni/Au = 100/30/100 nm) and p-type (Cr/Au = 20/100 nm) ohmic contacts were formed by electron beam evaporation and liftoff processes. Selective etching of the sacrificial layer (*i.e.*, AlAs) was performed in HCl/H_2O (3:1 by volume) with a photoresist anchor structure.[33] The undercut-etched microcells were then released by an elastomeric stamp made of polydimethylsiloxane (PDMS, Sylguard 184, Dow Corning), in which the exposed bottom contact was wet-chemically etched in $C_6H_8O_7/H_2O_2$ (4:1 by volume) to decrease the thickness from ~1300 to ~270 nm. Last, the retrieved microcells were printed on a glass or PET substrate using a photocurable adhesive (~1 μm).[34] More details of the fabrication processes are available in the Supporting Information.

Optical and Photovoltaic Characterization of GaAs Solar Microcells. The reflection and transmission spectra were measured by a homemade optical setup consisting of a white light source and fiber-optic spectrometer (USB 4000, Ocean Optics). A fiber-coupled light source was collimated by an achromatic doublet lens (f = 19 mm, N.A. = 0.42) and subsequently focused on the cell region (beam diameter = ~50 μm) through an objective lens (50×, N.A. = 0.4). The reflected light was gathered by the same objective lens and guided to the spectrometer through a multimode fiber, whereas the transmitted light was collected by another objective lens (10×, N.A. = 0.26). As a 100% calibration standard, a silver mirror and a transparent substrate coated with a printing medium were employed in reflectance and transmittance measurements, respectively. The photovoltaic performance was characterized using a semiconductor parameter analyzer (4156C, Agilent Technologies) and a full-spectrum solar simulator (94042A, Oriel). For photovoltaic measurements of flexible modules, cylindrical supports were used to define the bending radii, where microcells at the center of the arrays were illuminated at a normal incidence angle.

Optical and Electrical Modeling of GaAs Solar Cells. Optical simulation for GaAs solar cells with front-surface dielectric nanostructures was implemented through the FDTD method (FDTD Solutions 8, Lumerical Solutions). A 3D simulation volume comprising epitaxial layers identical to the experimental GaAs solar cell was defined, where periodic boundary condition in x- and y-directions and 'perfectly matched layers (PML)' boundary condition in z-direction were applied. A continuous plane-wave source with a broad Gaussian frequency spectrum (330−750 THz) was normally incident in (−)z-direction to the simulation volume. On the basis of the calculated electric field ($\vec{E}$), distribution of absorbed power per unit volume (p_{abs}) normalized by the source power (P_s) was obtained. Electrical simulation for GaAs solar cells was conducted with FEM-based software (DEVICE 4.5, Lumerical Solutions), where the same layer specifications as those in the experimental system was implemented. To calculate the short-circuit current density generated by optical absorption in constituent layers, distribution of the number of generated electron−hole pairs per unit volume and time ($g_{e\text{-}h}$) under AM1.5G standard solar illumination was calculated by $g_{e\text{-}h}(r) = \int[(\lambda/hc)(p_{abs}(r,\lambda)/P_s)I_{1.5G}(\lambda)S_{inc}]\ d\lambda$ (h, Planck's constant; $I_{1.5G}$, standard AM1.5G solar irradiance; S_{inc}, illumination area) using the FDTD optical simulation, and subsequently imported into the FEM device simulator, with assumptions including unity quantum efficiency, room temperature operation, Auger and radiative recombination, and perfect ohmic contacts. Details of material constants used in optical and electrical simulations are available in the Supporting Information (Figure S2, Table S1).

Conflict of Interest: The authors declare no competing financial interest.

Acknowledgment. The parts of the work involving fabrication of photovoltaic cells and modules, and optical modeling were supported by the National Science Foundation under Grant No (ECCS-1202522, ECCS-1509897) and DARPA YFA program (N66001-12-1-4244), respectively. The authors thank the Center for Energy Nanoscience at USC for the use of spectrophotometer, Donghai Zhu and John Curulli for help using facilities at Keck photonics laboratory and center for electron microscope and microanalysis (CEMMA) at USC, respectively.

Supporting Information Available: The Supporting Information is available free of charge on the ACS Publications website at DOI: 10.1021/acsnano.5b05585.

Additional methods for sample fabrication; notes for cost analysis; additional figures and legends (Figure S1−S22), details of experiments and calculations; additional Tables (Table S1−S3), material constants used in simulations, details of photovoltaic performance (PDF)

REFERENCES AND NOTES

1. Philipps, S. P.; Hoheisel, R.; Gandy, T.; Stetter, D.; Hermle, M.; Dimroth, F.; Bett, A. W. In *An Experimental and Theoretical Study on the Temperature Dependence of GaAs Solar Cells*, Photovoltaic Specialists Conference (PVSC), 2011, 37th IEEE, 19−24 June 2011; IEEE: New York, 2011; pp 001610−001614.
2. Ponce-Alcantara, S.; Connolly, J. P.; Sanchez, G.; Miguez, J. M.; Hoffmann, V.; Ordas, R. A Statistical Analysis of the Temperature Coefficients of Industrial Silicon Solar Cells. *Energy Procedia* **2014**, *55*, 578–588.
3. Blakemore, J. Semiconducting and Other Major Properties of Gallium Arsenide. *J. Appl. Phys.* **1982**, *53*, R123–R181.
4. Adachi, S. *GaAs and Related Materials: Bulk Semiconducting and Superlattice Properties*; World Scientific: River Edge, NJ, 1994.
5. Adachi, S. Optical Properties. In *Physical Properties of III-V Semiconductor Compounds*; Wiley-VCH Verlag GmbH & Co. KGaA: New York, 2005; pp 135−192.
6. Yamaguchi, M.; Takamoto, T.; Araki, K.; Ekins-Daukes, N. Multi-Junction III-V Solar Cells: Current Status and Future Potential. *Sol. Energy* **2005**, *79*, 78–85.
7. Dimroth, F. High-efficiency solar cells from III-V compound semiconductors. In *Physica Status Solidi C—Current Topics in Solid State Physics*; Stutzmann, M., Ed.; Wiley-Vch, Inc.: New York, 2006; Vol. 3, no. 3, pp 373−379.
8. vanGeelen, A.; Hageman, P. R.; Bauhuis, G. J.; vanRijsingen, P. C.; Schmidt, P.; Giling, L. J. Epitaxial Lift-Off GaAs Solar Cell from a Reusable GaAs Substrate. *Mater. Sci. Eng., B* **1997**, *45*, 162–171.
9. Cotal, H.; Fetzer, C.; Boisvert, J.; Kinsey, G.; King, R.; Hebert, P.; Yoon, H.; Karam, N. III-V Multijunction Solar Cells for Concentrating Photovoltaics. *Energy Environ. Sci.* **2009**, *2*, 174–192.
10. Yoon, J.; Jo, S.; Chun, I. S.; Jung, I.; Kim, H. S.; Meitl, M.; Menard, E.; Li, X. L.; Coleman, J. J.; Paik, U.; Rogers, J. A. GaAs Photovoltaics and Optoelectronics Using Releasable Multilayer Epitaxial Assemblies. *Nature* **2010**, *465*, 329–U80.
11. Kang, D. S.; Arab, S.; Cronin, S. B.; Li, X. L.; Rogers, J. A.; Yoon, J. Carbon-Doped GaAs Single Junction Solar Microcells Grown in Multilayer Epitaxial Assemblies. *Appl. Phys. Lett.* **2013**, *102*, 253902.
12. Choi, W.; Kim, C. Z.; Kim, C. S.; Heo, W.; Joo, T.; Ryu, S. Y.; Kim, H.; Kim, H.; Kang, H. K.; Jo, S. A Repeatable Epitaxial Lift-Off Process from a Single GaAs Substrate for Low-Cost and High-Efficiency III-V Solar Cells. *Adv. Energy Mater.* **2014**, *4*, 1400589.
13. Vandamme, N.; Chen, H.-L.; Gaucher, A.; Behaghel, B.; Lemaitre, A.; Cattoni, A.; Dupuis, C.; Bardou, N.; Guillemoles, J. F.; Collin, S. Ultrathin GaAs Solar Cells With a Silver Back Mirror. *IEEE J. Photovolt.* **2015**, *5*, 565–570.
14. Yang, W.; Becker, J.; Liu, S.; Kuo, Y.-S.; Li, J.-J.; Landini, B.; Campman, K.; Zhang, Y.-H. Ultra-Thin GaAs Single-Junction Solar Cells Integrated with a Reflective Back Scattering Layer. *J. Appl. Phys.* **2014**, *115*, 203105.
15. Nakayama, K.; Tanabe, K.; Atwater, H. A. Plasmonic Nanoparticle Enhanced Light Absorption in GaAs Solar Cells. *Appl. Phys. Lett.* **2008**, *93*, 121904.
16. Sheng, X.; Shen, L.; Kim, T.; Li, L. F.; Wang, X. R.; Dowdy, R.; Froeter, P.; Shigeta, K.; Li, X. L.; Nuzzo, R. G.; Giebink, N. C.; Rogers, J. A. Doubling the Power Output of Bifacial Thin-Film GaAs Solar Cells by Embedding Them in Luminescent Waveguides. *Adv. Energy Mater.* **2013**, *3*, 991–996.
17. Shir, D.; Yoon, J.; Chanda, D.; Ryu, J. H.; Rogers, J. A. Performance of Ultrathin Silicon Solar Microcells with Nanostructures of Relief Formed by Soft Imprint Lithography for Broad Band Absorption Enhancement. *Nano Lett.* **2010**, *10*, 3041–3046.
18. Yu, K. J.; Gao, L.; Park, J. S.; Lee, Y. R.; Corcoran, C. J.; Nuzzo, R. G.; Chanda, D.; Rogers, J. A. Light Trapping in Ultrathin Monocrystalline Silicon Solar Cells. *Adv. Energy Mater.* **2013**, *3*, 1401–1406.
19. Lee, S. M.; Biswas, R.; Li, W. G.; Kang, D.; Chan, L.; Yoon, J. Printable Nanostructured Silicon Solar Cells for High-Performance, Large-Area Flexible Photovoltaics. *ACS Nano* **2014**, *8*, 10507–10516.
20. Jeong, S.; McGehee, M. D.; Cui, Y. All-Back-Contact Ultrathin Silicon Nanocone Solar Cells with 13.7% Power Conversion Efficiency. *Nat. Commun.* **2013**, *4*, 2950.
21. Hsu, C. M.; Battaglia, C.; Pahud, C.; Ruan, Z. C.; Haug, F. J.; Fan, S. H.; Ballif, C.; Cui, Y. High-Efficiency Amorphous Silicon Solar Cell on a Periodic Nanocone Back Reflector. *Adv. Energy Mater.* **2012**, *2*, 628–633.
22. Ferry, V. E.; Verschuuren, M. A.; Li, H.; Schropp, R. E. I.; Atwater, H. A.; Polman, A. Improved Red-Response in Thin Film a-Si:H Solar Cells with Soft-Imprinted Plasmonic Back Reflectors. *Appl. Phys. Lett.* **2009**, *95*, 183503.
23. Chan, L.; Kang, D.; Lee, S. M.; Li, W. G.; Hunter, H.; Yoon, J. Broadband Antireflection and Absorption Enhancement of Ultrathin Silicon Solar Microcells Enabled with Density-Graded Surface Nanostructures. *Appl. Phys. Lett.* **2014**, *104*, 223905.
24. delValle, C. A.; Alcaraz, M. F. Performance of Antireflecting Coating-AlGaAs Window Layer Coupling for Terrestrial Concentrator GaAs Solar Cells. *IEEE Trans. Electron Devices* **1997**, *44*, 1499–1506.
25. Plá, J.; Barrera, M.; Rubinelli, F. The Influence of the InGaP Window Layer on the Optical and Electrical Performance of GaAs Solar Cells. *Semicond. Sci. Technol.* **2007**, *22*, 1122.
26. Yu, P.; Chang, C.-H.; Chiu, C.-H.; Yang, C.-S.; Yu, J.-C.; Kuo, H.-C.; Hsu, S.-H.; Chang, Y.-C. Efficiency Enhancement of GaAs Photovoltaics Employing Antireflective Indium Tin Oxide Nanocolumns. *Adv. Mater.* **2009**, *21*, 1618–1621.
27. Liang, D.; Kang, Y.; Huo, Y.; Chen, Y.; Cui, Y.; Harris, J. S. High-Efficiency Nanostructured Window GaAs Solar Cells. *Nano Lett.* **2013**, *13*, 4850–4856.
28. Leem, J. W.; Su, Y. J.; Jun, D.-H.; Heo, J.; Park, W.-K. Efficiency Improvement of III−V GaAs Solar Cells Using Biomimetic TiO_2 Subwavelength Structures with Wide-Angle and Broadband Antireflection Properties. *Sol. Energy Mater. Sol. Cells* **2014**, *127*, 43–49.
29. Wallentin, J.; Anttu, N.; Asoli, D.; Huffman, M.; Aberg, I.; Magnusson, M. H.; Siefer, G.; Fuss-Kailuweit, P.; Dimroth, F.; Witzigmann, B.; Xu, H. Q.; Samuelson, L.; Deppert, K.; Borgstrom, M. T. InP Nanowire Array Solar Cells Achieving 13.8% Efficiency by Exceeding the Ray Optics Limit. *Science* **2013**, *339*, 1057–1060.
30. Kayes, B. M.; Hui, N.; Twist, R.; Spruytte, S. G.; Reinhardt, F.; Kizilyalli, I. C.; Higashi, G. S. *27.6% Conversion Efficiency, A New Record for Single-Junction Solar Cells under 1 Sun Illumination*, Photovoltaic Specialists Conference (PVSC), 2011 37th IEEE; 19−24 June 2011; IEEE: New York, 2011; pp 000004−000008.
31. Steiner, M. A.; Geisz, J. F.; Garcia, I.; Friedman, D. J.; Duda, A.; Kurtz, S. R. Optical Enhancement of the Open-Circuit Voltage in High Quality GaAs Solar Cells. *J. Appl. Phys.* **2013**, *113*, 123109.
32. Kang, D.; Lee, S. M.; Li, Z. W.; Seyedi, A.; O'Brien, J.; Xiao, J. L.; Yoon, J. Compliant, Heterogeneously Integrated GaAs Micro-VCSELs towards Wearable and Implantable Integrated Optoelectronics Platforms. *Adv. Opt. Mater.* **2014**, *2*, 373–381.
33. Kang, D.; Lee, S.-M.; Kwong, A.; Yoon, J. Dramatically Enhanced Performance of Flexible Micro-VCSELs via Thermally Engineered Heterogeneous Composite Assemblies. *Adv. Opt. Mater.* **2015**, *3*, 1072–1078.
34. Kim, T. I.; Kim, M. J.; Jung, Y. H.; Jang, H.; Dagdeviren, C.; Pao, H. A.; Cho, S. J.; Carlson, A.; Yu, K. J.; Ameen, A.; Chung, H. J.; Jin, S. H.; Ma, Z. Q.; Rogers, J. A. Thin Film Receiver Materials for Deterministic Assembly by Transfer Printing. *Chem. Mater.* **2014**, *26*, 3502–3507.
35. Rogers, J. A.; Lagally, M. G.; Nuzzo, R. G. Synthesis, Assembly and Applications of Semiconductor Nanomembranes. *Nature* **2011**, *477*, 45–53.